Sādhanā (2020)45:147
https://doi.org/10.1007/s12046-020-01389-z

Comparative analysis of new improved force split-teeth Linear Switched Reluctance Motor for high speed transit systems

NISHA PRASAD[1,*], SHAILENDRA JAIN[1,2] and SUSHMA GUPTA[1]

[1]Department of Electrical Engineering, Maulana Azad National Institute of Technology, Bhopal, MP, India
[2]Sant Longowal Institute of Engineering and Technology, Longowal, Punjab, India
e-mail: nipr24@gmail.com; sjain68@gmail.com; sush_gupta@yahoo.com

MS received 29 May 2019; revised 3 February 2020; accepted 23 April 2020

Abstract. Linear Motors forms an integral part of propulsion systems used in linear motor propelled high-speed transport systems. Generally, motors such as linear induction and linear synchronous are preferred worldwide for these applications. In spite of showing the immense capabilities, linear switched reluctance motor (LSRM) is still under research for applications in high-speed systems. This paper focuses on a LSRM with enhanced propulsion force for the application in high-speed transportation systems. It has a linear structure with moving translator for direct force transmission and two-teeth in each stator pole to attain better force performance. In the proposed motor, translator teeth count is more as compared to the stator teeth count. A 6/16 LSRM with three- phase split-teeth stator has been proposed. The performance of the proposed 6/16 LSRM has been compared with 6/4 and 6/8 three-phase conventional motors to highlight the improvements in the proposed motor. The paper also modifies the proposed 6/16 LSRM into 12/32 configuration to analyse its force ripple reduction capability. The performance of the 6/16 is compared with the 12/32 LSRM. All the motors are modelled and analysed in 3D with the help of finite-element analysis (FEA). The paper optimizes the 6/16 LSRM using parameter based cumulative deterministic optimization algorithm (PBCDOA) to maximize its propulsion force. The FEA based analysis shows better force performance for the proposed motor.

Keywords. Linear switched reluctance motor; force ripple; propulsion force; parameter optimization; finite element analysis; high speed applications.

1. Introduction

Linear motor propelled high-speed transportation systems are increasing their proportion since the past few decades to cope-up with the worsening transport crisis due to rising urbanization [1]. Improvement in efficiency of such systems involves optimization of many of its components including power source, propulsion motors, drive control circuit, its dimensions and weight [2].

Linear motors constitute the important part of these transportation systems. These motors not only propel the vehicle, but they also impart the required braking force to the system. Therefore, better performance motors become a necessity for these systems [3]. Generally, motors like linear synchronous and linear induction are preferred for such applications [4].

However, Linear switched reluctance motors (LSRMs) have been under research because of their inherent advantages of low cost, high fault immunity, extensive speed range, robust structure and absence of permanent magnets. These features make LSRM a potential candidate for high-speed transit systems [5]. But, double saliency and high flux saturation in the stator and translator steel make the LSRM highly non-linear that leads to poor efficiency and inferior force performance of the machine [6].

LSRM can be broadly classified into longitudinal flux and transverse flux motors based upon the flux direction in comparison with the direction of motion [6, 7]. The longitudinal LSRMs that involve flux movement parallel to that with the plane of movement are generally chosen for transport applications. The Longitudinal LSRM can be divided into moving stator LSRM and moving translator LSRM. Both of these topologies have their own merits and demerits. Moving stator LSRM when used in transit systems, the stator travels along with the vehicle whereas translator lays on the ground to form the part of the track. In this configuration in-housed windings of the stator raises the control requirement, vehicle dimensions and weight. On the other hand, the translator simplifies the track model. Nevertheless, LSRM with moving translator decreases the vehicle weight at the price of high initial track construction cost. However, this configuration is generally recommended for high-speed applications due to its suitability for direct force transmission that decreases the mechanical gear requirements.

*For correspondence
Published online: 04 June 2020

Available literature contains various types of LSRM designs in both transverse flux and longitudinal flux forms [5–7]. Researchers generally follow a common design procedure for longitudinal LSRM involving calculation of linear dimensions from equivalent rotary dimensions as presented in [8]. Many designs of linear and rotating SRMs include multi-teeth construction in the motor to improve its performance characteristics [9–12]. A planar SRM with multi-teeth stator has been presented in [9]. However, this design is not suitable for transit applications as it requires additional design arrangements to fix the stator on the vehicle. Also, stator design has not provided any benefit in increasing the slot area. A multi-teeth skewed stator is presented in [10]. This design is presented for reducing the noise reduction in the LSRM. Multi-teeth stator structure for rotary SRM is presented in [11, 12]. The structure presented in [11] has shown to improve both torque density and fault tolerant capability of the rotary SRM. While, double-teeth stator structure presented in [12] shows the enhancement inefficiency, torque ripples and specific torque of the rotary SRM. But due to suitability of linear motors in high-speed applications, this multi-teeth design has been implemented and studied for LSRM in this work.

This paper presents a new LSRM, with two teeth in each stator pole. This design contains increased number of teeth in translator as compared to teeth in stator. Using more translator teeth widens the slot size, which becomes helpful in accommodating more copper per phase if required. Increased slot area also improves the maintenance and cooling of the stator windings. However, this may increase the volume and initial stator cost because of the extra steel. But, this extra weight enhances the mechanical strength of the stator.

The paper gives a FEA based detailed analysis of field and force characteristics of the proposed 6/16 LSRM. The improvement in its performance is highlighted by comparing it with three-phase 6/4 and 6/8 conventional LSRM designed for the similar stack dimensions. Further, the force ripples reduction capability of the 6/16 LSRM (proposed motor) is tested by converting its configuration into a 12/32 LSRM. The static and dynamic force characteristics are determined and analysed by using FEA software. Finally, the proposed motor is subjected to optimization using parameter based cumulative deterministic optimization algorithm (PBCDOA) to further enhance its force performance [13].

The paper contains 5 sections. The second section illustrates the operating principle, design parameters and topology of the proposed motor. It consists of 3 subsections which give details regarding the magnetic characteristics of the proposed 6/16 LSRM. To feature the eminence of the proposed 6/16 LSRM, its characteristics are quantitatively studied in comparison with 6/4 and 6/8 conventional LSRMs simulation models developed for similar stack dimensions. To test the force ripple reduction capability of the 6/16 proposed motor, it is also designed with 12/32 configuration. The details of these motors are given in section 2. Parameter based cumulative deterministic optimization algorithm is applied to the proposed LSRM to improve its force performance. Section 3 discusses this algorithm in detail. It also presents comparison between optimized motor performances with non-optimized motor. Section 4 discusses about the performance comparison of the proposed LSRM with the other designed LSRMs and conclusion is presented in section 5.

2. Features of LSRM

LSRMs consist of two main parts namely stator and translator. To accomplish this study four LSRMs with moving translator have been designed and investigated. Figure 1 shows the structural comparison between the designed LSRMs.

2.1 *Operating principle*

Due to its double-salient structure, the LSRM always traces the minimum reluctance position for its working.

Whenever a phase is excited in the motor, the translator and stator teeth tries to attain the position of minimum

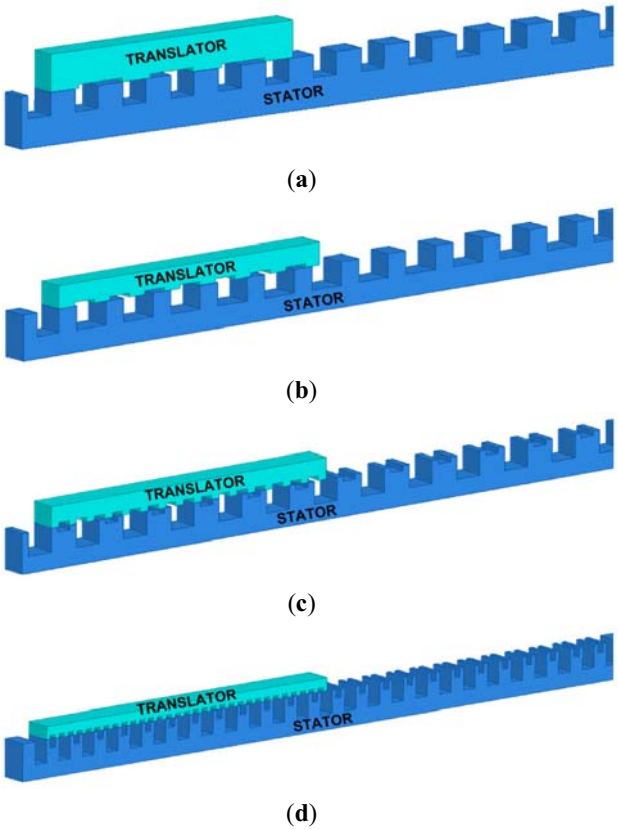

Figure 1. Structural details (**a**) 6/4 LSRM, (**b**) 6/8 LSRM, (**c**) Proposed 6/16 LSRM and (**d**) 12/32LSRM.

reluctance. While doing that, moving part of the motor shifts from non-aligned position to aligned position. Magnetic flux paths are utilized to explain the working principle of the LSRM.

Figure 2 shows the flux paths during different teeth positions. At aligned position, translator teeth align themselves with the excited stator teeth to minimize the flux path reluctance. Lowest reluctance position corresponds to the maximum inductance at that particular position. Figure 3 shows the flux path of the conventional and proposed LSRMs at aligned teeth position.

2.2 *Magnetic characteristics of LSRM*

The propulsion force generated by the LSRM greatly depends on the reluctance and flux variation due its double-saliency. The equivalent circuit per phase of the LSRM is given as Eq. (1) when the excitation voltage/ phase is V, resistance/phase is R, excitation current/phase is i and total flux linkage/phase is ψ.

$$V = Ri + \frac{d}{dt}(\psi) \tag{1}$$

Flux linkage/phase (ψ) is given as Eq. (2), when turns/phase is N, flux/phase is ø, winding inductance/phase is L and x represents the translator position.

$$\psi = N\text{ø} = L(x,i) * i \tag{2}$$

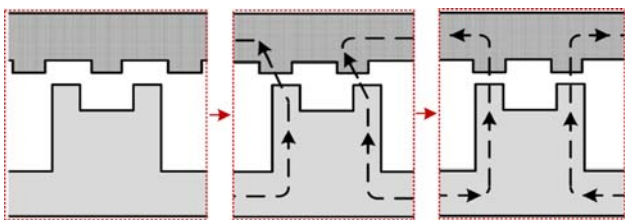

Figure 2. Operating principle LSRM (**a**) non-aligned position, (**b**) half-aligned position and (**c**) aligned position.

However, gross flux /phase consist of ø_m (magnetizing flux) and ø_l (leakage flux).

$$\text{ø} = \text{ø}_m + \text{ø}_l \tag{3}$$

Using Eq. (2), Eq. (1) is modified as:

$$V = Ri + \frac{d}{dt}(L(x,i) * i) \tag{4}$$

On Multiplication of i on both sides of Eq. (4), power equation is formed as Eq. (5).

$$Vi = Ri^2 + i * \frac{d}{dt}(L(x,i) * i) \tag{5}$$

Reorganizing the data in power equation gives Eqs. (6) and (7) to show the power usage of the LSRM.

$$Vi = Ri^2 + \frac{1}{2}i^2\frac{dx}{dt}\frac{dL(x,i)}{dx} + \frac{d}{dt}\left(\frac{1}{2}i^2 * L(x,i)\right) \tag{6}$$

$$Vi = Ri^2 + \frac{1}{2}i^2 v_s\frac{dL(x,i)}{dx} + \frac{d}{dt}\left(\frac{1}{2}i^2 * L(x,i)\right) \tag{7}$$

where v_s is the translator speed. In Eq. (7), first, second and third term represent the losses in copper/phase, the power generated by the LSRM/phase (P_m) and the energy stored in the winding inductance/phase respectively, assuming no saturation in the core.

Therefore, from Eq. (7) mechanical power developed per phase is written as:

$$P_m = \frac{1}{2}i^2 v_s\frac{dL(x,i)}{dx} = F_m v_s \tag{8}$$

where, generated propulsion force is given as F_m .Therefore assuming no saturation in the core, propulsion force generated by the LSRM is obtained from Eq. (8) as:

$$F_m = \frac{1}{2}i^2\frac{dL(x,i)}{dx} \tag{9}$$

Now L(x,i) is also given as Eq. (10), when total magnetic field path reluctance is given as S. The S comprises of air-gap reluctance (S_g) and iron path reluctance (S_i).

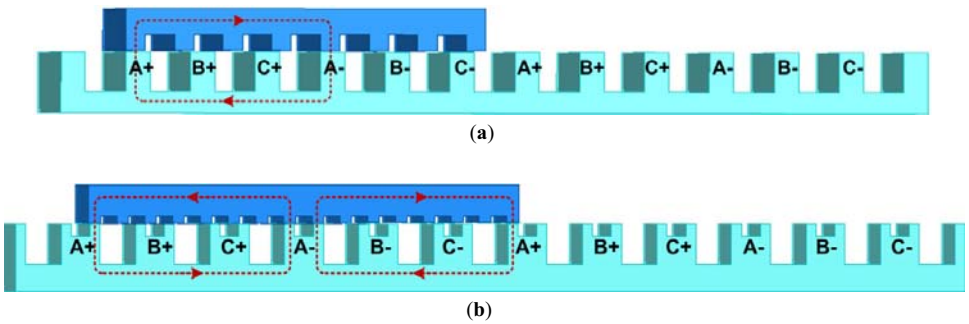

Figure 3. Flux path during aligned teeth position (**a**) Conventional LSRM. (**b**) Proposed LSRM.

$$L(x,i) = \frac{N^2}{S} = \frac{N^2}{S_g + S_i} = \frac{N^2}{S_g}, \quad \text{as } S_g \gg S_i \tag{10}$$

where

$$S_i = \frac{l_i}{\mu_o \mu_r A_i} \tag{11a}$$

$$S_g = \frac{l_g}{\mu_o n\ A_g} = \frac{l_g}{\mu_o n l_{lap}(x) L_s} \tag{11b}$$

where l_i and l_g are lengths of iron path and air-gap, respectively. Whereas, A_i and A_g are cross-sectional areas of iron-path and air-gap, respectively. The relative permittivity of the core material and permeability are given as μ_r and μ_o respectively, teeth count/ pole is n, the stack length is L_s and the overlap span between the translator and stator teeth is $l_{lap}(x)$, which varies with position x. From Eqs. (9), (10) and (11), propulsion force developed by the LSRM is calculated as Eq. (12).

$$F_m = \frac{1}{2} i^2 \frac{d}{dx} \left\{ \frac{\mu_o n N^2 l_{lap}(x) L_s}{l_g} \right\} \tag{12}$$

Eq. (10) and (11) show that the inductance of the LSRM is a function of position (x) because of the dependency of reluctance on the comparative position of stator and translator. Similarly as shown by Eq. (12), propulsion force of the LSRM is also a function of position (x). Therefore, this paper gives a FEA software based technique to find the value of changing phase inductances and propulsion force of the LSRM at each and every position of the translator, as the motor starts moving from one position to another. The use of this software thus reduces the need of such complicated analytical calculations.

2.3 *Machine configurations*

To feature the capabilities of proposed LSRM, two conventional LSRMs with 4 and 8 translator teeth configuration have been designed and compared with the 16 translator teeth proposed LSRM. Conventional LSRMs are designed for same stack dimensions as used for designing the 6/16 proposed LSRM. The proposed LSRM translator is further divided into 32 teeth to form the 12/32 configuration of proposed LSRM. The performance of 12/32 LSRM is compared with the 6/16 LSRM to test its force ripple reducing capability. All the designed motors in this study comprise of short moving translator that forms the part of the moving vehicle while stator forms the stationary track for the moving vehicle .Stator of these motors contains the three-phase concentric windings made of copper.

Stator and translators of the motors consist only of ferromagnetic steel material having non-linear B-H characteristics. Translator of the proposed LSRM contains 16 teeth. Further, the design of proposed LSRM is altered by adding 32 teeth in its translator that decrease its translator pole pitch accordingly. In this modified 12/32 LSRM, each stator phase contains 4 stator poles. Motor stators have same slot fill factor of 0.54 with same number of turns per phase that are excited using the winding current of same magnitude. All the motors are designed for same stack dimensions. Figure 4 represents the various design dimensions used for designing the LSRMs.

These design parameters are calculated using the same procedure of converting rotary dimensions into linear dimensions given in ref. [13]. The number of stator phases are kept same in the designed LSRMs to keep the converter requirements same. Only the number of translator teeth is increased in the designed motors and its effect has been studied on the force performance of the motor. Table 1 lists

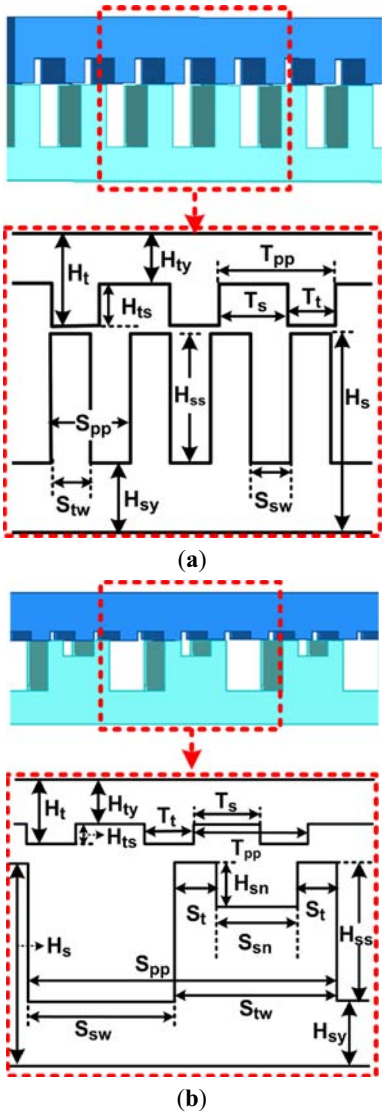

Figure 4. Design dimensions (**a**) Conventional LSRM, (**b**) Proposed LSRM.

Table 1. Physical parameters of the designed LSRM.

S. no.	Parameters	6/4 LSRM	6/8 LSRM	6/16 LSRM	12/32 LSRM
1.	Stack length (L_s) (mm)	74	74	74	74
2.	Breadth stator teeth (S_{tw}) mm)	81.4	58.5	81.4	41.2
3.	Breadth stator slot (S_{sw}) (mm)	74.6	97.5	74.6	36.8
4.	Height Stator teeth (H_{ss}) (mm)	62.4	62.4	62.4	62.4
5.	Height stator yoke (H_{sy}) (mm)	81.4	58.5	41.6	41
6.	Pole-pitch stator (S_{pp}) (mm)	156	156	156	78
7.	Height stator (H_s) (mm)	143.8	120.9	104	103.4
8.	Breadth translator teeth (t_t) (mm)	92	50.8	23	12
9.	Breadth translator slot (t_s) (mm)	141.6	66	35.4	17.2
10.	Height translator teeth (h_{ts}) (mm)	10	10	10	10
11.	Height translator yoke (h_{ty}) (mm)	92	50.8	48	24
12.	Height translator (h_t) (mm)	102	60.8	58	34
13.	Pole-pitch translator (t_{pp}) (mm)	233.6	116.8	58.4	29.2
14.	Length air-gap (l_g) (mm)	1	1	1	1
15.	Slot Fill-factor	0.54	0.54	0.54	0.54
16.	Turns count / phase (N) (nos.)	212	212	212	212
17.	Peak excitation current (A)	8.5	8.5	8.5	8.5

the different mechanical and electrical parameters used for the designing of conventional and proposed LSRMs.

3. Parameter based cumulative deterministic optimization of proposed LSRM

The average propulsion force and ripples in the propulsion force generally measure the propulsion force performance of the LSRM. This paper analyses all the designed motors. However, since proposed LSRM contains a stator design modification due to addition of a notch therefore the designed dimensions of the 6/16 LSRM are further corrected with parameter based cumulative deterministic optimization algorithm (PBCDOA) [13]. To start the optimization process, initially the LSRM is designed with 16 translator teeth having no stator notch. However, the breadth of the stator teeth was increased to maintain the number of stator phases constant.

Figure 5 shows the structural difference between the LSRM with zero stator notch and LSRM with notch. For further reference, LSRM without notch will be referred as LSRM (0) and un-optimized LSRM with notch will be referred as LSRM (1).

Fill-factor of the slot, turns count/phase, heights of stator and translator, pole-pitches of stator and translator, air-gap, and stack length are maintained constant during the entire optimization. Figure 6 shows the algorithm used for the optimization process.

Table 2 shows force performance comparison of the conventional LSRMs and LSRM (0). The LSRM (0) with no addition of stator notch gives poor force performance with inferior force magnitude and higher ripples in force in comparison with the conventional 6/4 and 6/8 LSRMs.

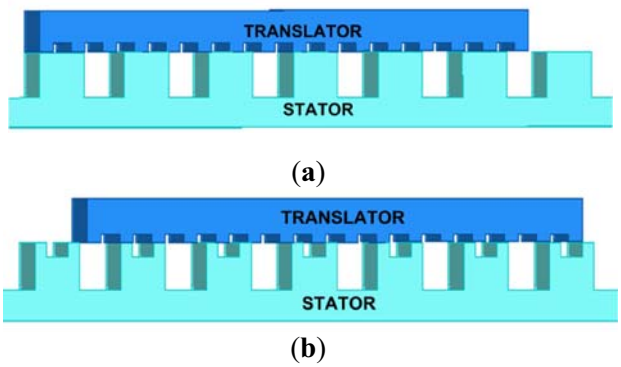

Figure 5. Basic structure (**a**) Stator with no notch, (**b**) Stator with notch.

To further increase the performance of the proposed LSRM stator notch of random dimensions is added to form LSRM (I) and the height of the stator notch is chosen as the first parameter to be optimized. At the various stages of optimization, priority has been given to the value of gross propulsion force as compared to the force ripple while selecting the optimised values for the parameters.

3.1 *Optimizing stator notch height (H_{sn})*

Firstly, the notch height in stator (H_{sn}) is optimized to improve the characteristics of the LSRM. The notch height is changed maintaining constant stator height. Ratio between heights of stator notch and stator is termed as $k_{sht.}$

$$k_{sht} = \frac{H_{sn}}{H_s}, \quad 0.09 \leq k_{sht} \leq 0.24. \tag{13}$$

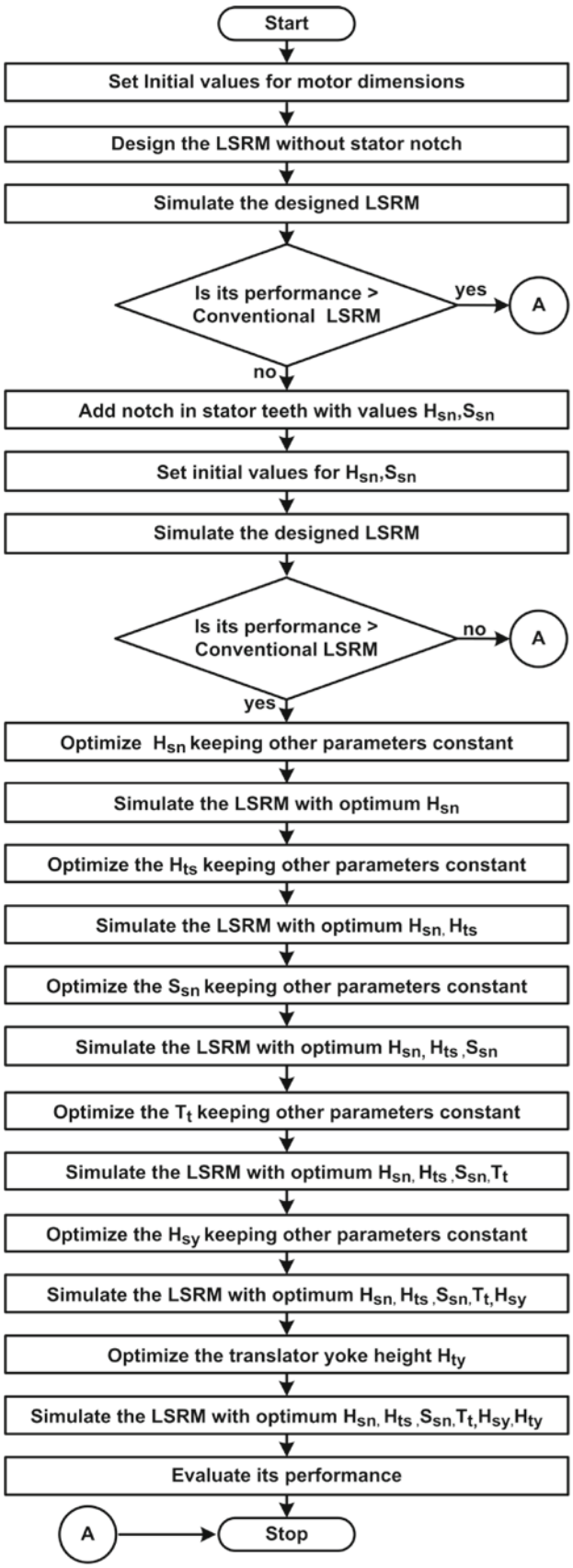

◀**Figure 6.** Parameter based cumulative deterministic optimization algorithm.

For maintaining the flux leakage from the windings within permissible limit, k_{sht} is chosen to vary within the ranges shown in Eq. (13). Effect of varying the height of stator notch on propulsion force and ripples produced by the LSRM (I) is shown in figure 7. Value of k_{sht} is chosen as 0.12 for optimizing the H_{sn}. Corresponding to this k_{sht}, H_{sn} is calculated as 13 mm using Eq. (13). The value of H_{sn} is changed to 13 mm in the design of LSRM (I), while maintaining the remaining parameters constant. The new motor so formed is termed as LSRM (II). This motor is designed and simulated. Table 3 gives the comparative analysis of LSRM (0) with LSRM (II) highlighting the effect of optimizing the stator notch height.

3.2 *Optimizing translator teeth height (H_{ts})*

After the first step, translator teeth height (H_{ts}) is chosen as a next parameter for optimization. For its accomplishment, H_{ts} is varied from 4 mm to 16 mm with the constant translator height of 58 mm. Ratio between heights of translator teeth and translator is given as $k_{tht.}$

$$k_{tht} = \frac{H_{ts}}{H_t}, \quad 0.06 \leq k_{tht} \leq 0.27 \tag{14}$$

The highest value of of k_{tht} is selected as 0.27 to maintain the translator yoke saturation with in limit. Whereas, the lowest value of k_{tht} is selected randomly, to start the optimization process. Impact of changing height of teeth in translator on the force characteristics of the LSRM (II) is shown in figure 8.

From the results shown in figure 8, the value of k_{tht} is optimized at 0.20. For this value of k_{tht}, H_{ts} is calculated as 12 mm using Eq. (14). By replacing the values of H_{sn} and H_{ts} with their optimum value in the LSRM (II) while retaining the other dimensions same, a refined motor is formed. This refined motor is termed as LSRM (III). In table 4, the performance of LSRM (II) is compared with LSRM (III) to highlight the effect of optimizing translator teeth height.

3.3 *Optimizing stator notch breadth (S_{sn})*

For additional enhancement, the stator notch breadth (S_{sn}) is chosen as the third parameter for optimization. For this study, S_{sn} has been varied within selected range for the constant stator teeth breadth of 81.4 mm as given in table 1.

The ratio between breadths of stator notch and stator teeth is termed as k_{swd} for this study.

Table 2. Performances at the beginning of the optimization.

S. no.	Features	6/4 LSRM	6/8 LSRM	LSRM (0)
1.	Gross propulsion force (N)	61.36	51.08	36.18
2.	Percentage ripple (%)	13.36	14.76	25.72

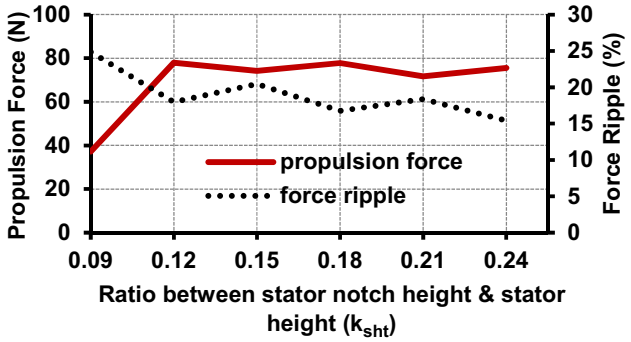

Figure 7. Performance variation with stator notch height.

Table 3. Performance comparison at stage 1.

S. no.	Features	LSRM (0)	LSRM (II)
1.	Gross propulsion force (N)	36.18	77.95
2.	Percentage ripple (%)	25.72	17.97

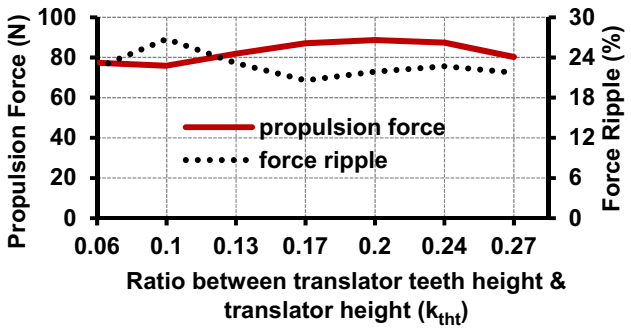

Figure 8. Performance variation with translator teeth height.

Table 4. Performance comparison at stage 2.

S. no.	Features	LSRM (II)	LSRM (III)
1.	Gross propulsion force (N)	77.95	88.38
2.	Percentage ripple (%)	17.97	17.16

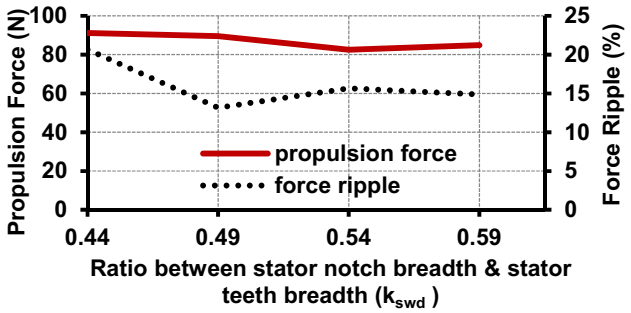

Figure 9. Performance variation with stator notch breadth.

$$k_{swd} = \frac{S_{sn}}{S_{tw}}, \quad 0.44 \le k_{swd} \le 0.59 \tag{15}$$

The value of k_{swd} has been ranged from 0.44 to 0.59, to retain the flux at the corners of stator teeth within permissible values. The effect of changing stator notch breadth (S_{sn}) on the force characteristics of the LSRM (III) is given in figure 9.

From results shown in figure 9, the value of 0.49 is chosen as the optimized value for k_{swd}. For this k_{swd}, the value of S_{sn} is calculated as 39.8 mm using Eq. (15).

By changing the values of H_{sn}, H_{ts} and S_{sn} with their optimized values in the LSRM (III) by retaining the other dimensions fixed, an enhanced LSRM is developed. This motor is termed as LSRM (IV). Table 5 presents the characteristics of LSRM (III) and LSRM (IV) to feature the effect of optimizing the stator notch breadth of the motor.

3.4 *Optimizing translator teeth breadth (T_t)*

As a next step, translator teeth breadth (T_t) is chosen for optimization. The characteristics of the LSRM is analysed for different values of T_t. For this, T_t is varied between 23 mm and 25 mm, for the constant value of translator pole-pitch. The range selection is done for maintaining the flux in the translator teeth within permissible values.

The ratio between breadths of translator teeth and pole-pitch is defined as k_{twd}.

$$k_{twd} = \frac{T_t}{T_{pp}}, \quad 0.39 \le k_{twd} \le 0.43 \tag{16}$$

Table 5. Performance comparison at stage 3.

S. no.	Features	LSRM (III)	LSRM (IV)
1.	Gross propulsion force (N)	88.38	88.99
2.	Percentage ripple (%)	17.16	15.38

Table 6. Performance comparison at stage 4.

S. no.	Features	LSRM (IV)	LSRM (V)
1.	Gross propulsion force (N)	88.99	90.65
2.	Percentage ripple (%)	15.38	15.17

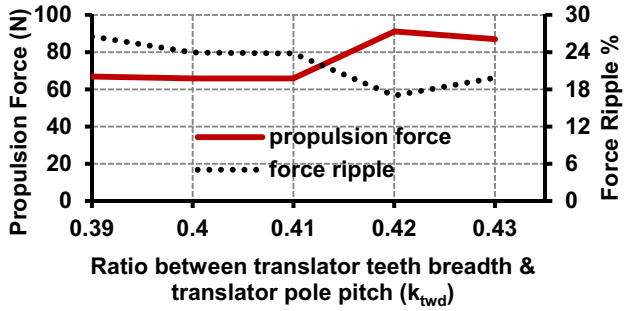

Figure 10. Performance variation with translator teeth breadth.

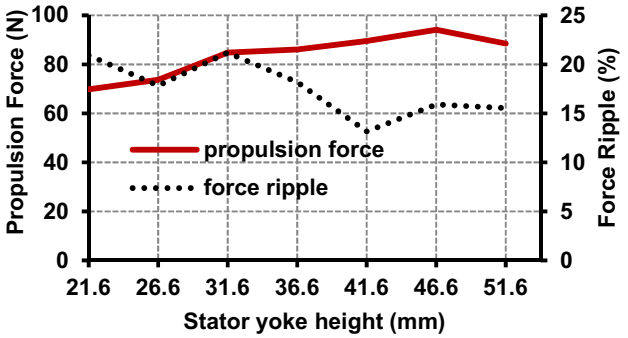

Figure 11. Performance variation with stator yoke height.

The values of T_t from 23 mm to 25 mm with constant value of 58.4 mm for the T_{pp}, gives the variation of k_{twd} from 0.39 to 0.43 using Eq. (16). Figure 10 shows the impact of changing the translator teeth breadth on the force characteristics of the LSRM (IV).

From the results shown in figure 10, optimum value of k_{twd} is chosen as 0.42. For this value of k_{twd}, T_t becomes equal to 24.5 mm using Eq. (16). By replacing the values of H_{sn}, H_{ts}, S_{sn} and T_t with their optimum values while retaining the remaining dimensions constant in the design of LSRM (IV), a refined LSRM is formed. This LSRM is termed as LSRM (V). Table 6 gives the comparative analysis of LSRM (V) with LSRM (IV) to highlight the effect of optimizing the translator teeth breadth.

3.5 *Optimizing stator yoke height (H_{sy})*

After 4 stages, stator yoke height (H_{sy}) is taken as a fifth parameter for optimization. The stator and translator yoke heights do not affect the force performance of the LSRM directly. They mainly impact the saturation in the core, which further affects the force characteristics of the motor. Thus, its performance is studied at different values of H_{sy}. To accomplish this study, H_{sy} is varied between the ranges of 21.6 mm to 51.6 mm.

For maintaining the saturation in the stator yoke with in limit, the lowest value of H_{sy} is taken as 21.6 while the highest value is selected randomly to end the optimization process. Figure 11 presents the impact of changing stator yoke height on the force characteristics of the LSRM (V). From the results, 46.6 mm value is selected as the optimized value for the H_{sy}.

Table 7. Performance comparison at stage 5.

S. no.	Features	LSRM (V)	LSRM (VI)
1.	Gross propulsion force (N)	90.65	91.12
2.	Percentage ripple (%)	15.17	20.66

Replacing the values of H_{sn}, H_{ts}, S_{sn}, T_t and H_{sy} with their optimum values in the design of LSRM (V) while maintaining the other dimensions fixed, a new LSRM (VI) is formed. Table 7 compares LSRM (VI) with LSRM (V) to highlight the effect of optimizing the stator yoke height.

3.6 *Optimizing translator yoke height (H_{ty})*

As a last step, translator yoke height (H_{ty}) is chosen for optimization. To achieve that, H_{ty} is varied from 28 mm to 53 mm. For retaining the flux values in translator yoke with in permissible range, the lowest value of H_{ty} is taken as 28 mm whereas highest value is selected arbitrarily to end the optimization process. Figure 12 gives the impact of varying H_{ty} on the force characteristics of the LSRM (VI).

Results shown in figure 12 give 46 mm as the optimum value for H_{ty}. Replacing the values of H_{sn}, H_{ts}, S_{sn}, T_t, H_{sy} and H_{ty} with their optimum values the final design of proposed 6/16 LSRM is obtained.

The comparative analysis of LSRM (VI) and the Proposed LSRM is given in table 8. The difference between the start and end values after the completion of optimization process is given in table 9.

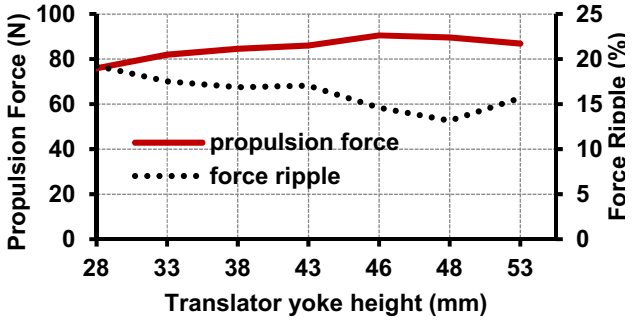

Figure 12. Performance variation with translator yoke height.

Table 8. Performance comparison at stage 6.

S. no.	Features	LSRM (VI)	Proposed LSRM
1.	Gross propulsion force (N)	91.12	96.31
2.	Percentage ripple (%)	20.66	15.91

4. Results and discussion

To highlight the superiority of the proposed split-teeth 6/16 LSRM, its characteristics is compared with two conventional 6/4 and 6/8 motors. All the designed motors are analysed using finite element analysis (FEA). The FEA based analysis gives detailed performance characteristics of any machine.

Therefore, field and force characteristics of all the three motors are studied using FEA. Under normal operating conditions, flux linkage profile, phase inductance profile, flux-current variation, flux density distribution, and force-current variation of the three LSRMs are compared and shown in figures 13–17.

To obtain these characteristics translator is set to travel a distance of 200 mm. Stator windings of all the motors are excited by constant current excitation of 8.5 A. The current excitation in each phase are set to energize the motor phase during rising inductance period of that particular phase. Figure 13 (a) represents the flux linkage per phase of the three motors whereas phase inductances variation of the three motors is shown by figure 13(b). Better flux linkage and phase inductance profiles have been shown by the proposed LSRM.

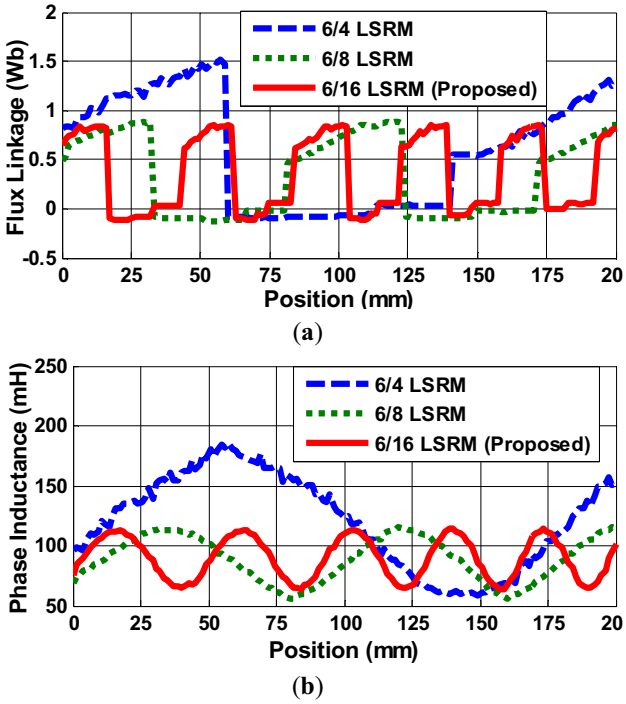

Figure 13. Comparison (**a**) Flux Linkage, (**b**) Inductance.

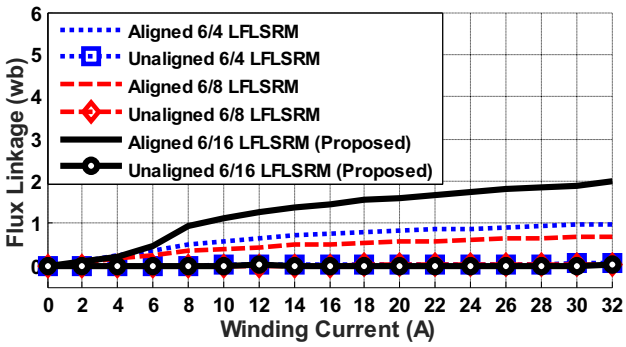

Figure 14. Flux current variation at aligned and non-aligned teeth position.

Table 9. Difference between start and end dimensions.

S. no.	Parameters	Initial value	Final value
1.	Stator notch height (H_{sn}) (mm)	0	13
2.	Translator teeth height ((H_{ts}) (mm)	10	12
3.	Stator notch breadth (S_{sn}) (mm)	0	39.8
4.	Translator teeth breadth (T_t) (mm)	23	24.5
5.	Stator yoke height (H_{sy}) (mm)	41.6	46.6
6.	Translator yoke height (H_{ty}) (mm)	48	46

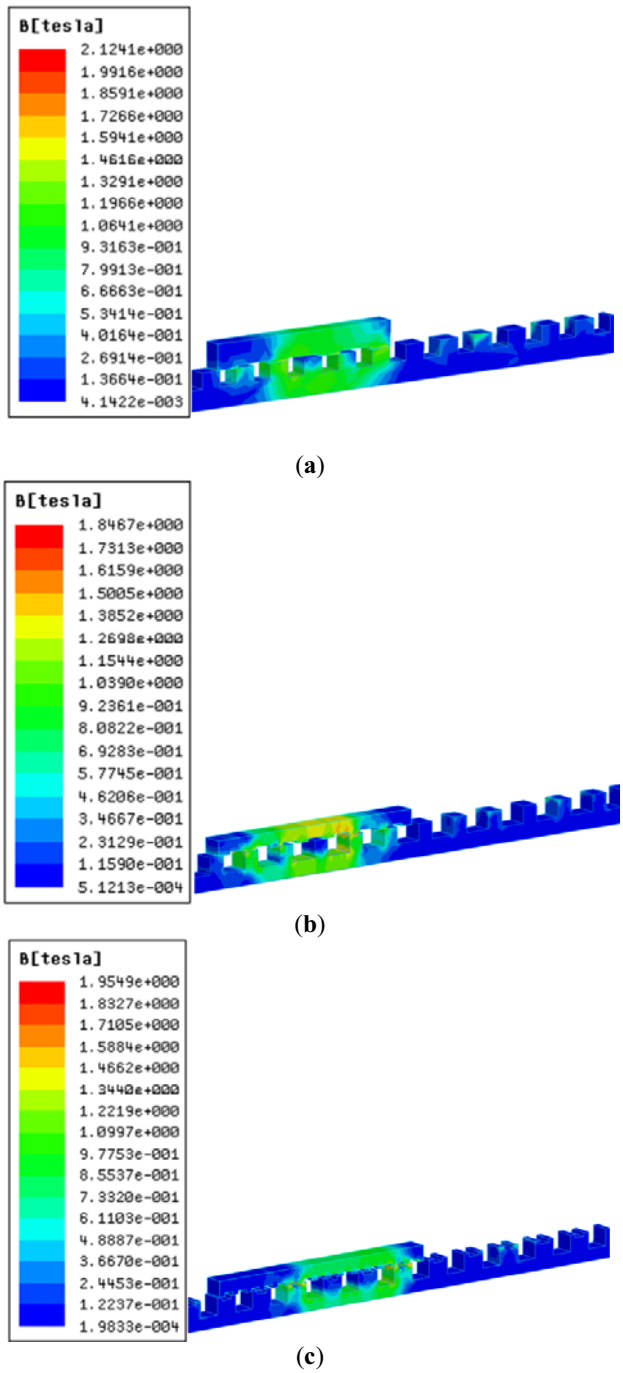

Figure 15. Flux density distribution (**a**) 6/4 LSRM, (**b**) 6/8 LSRM, (**c**) 6/16 LSRM (Proposed).

Increase in the difference between aligned and non-aligned inductances of the proposed LSRM leads to the improvement in its rate of change of inductance which further improves its force performance.

Figure 14 gives the variation of flux with current at aligned and non-aligned position. Varying the excitation current value gives the flux plot which is plotted as a function of current at aligned and non-aligned teeth positions of the designed motors. This figure clearly shows the

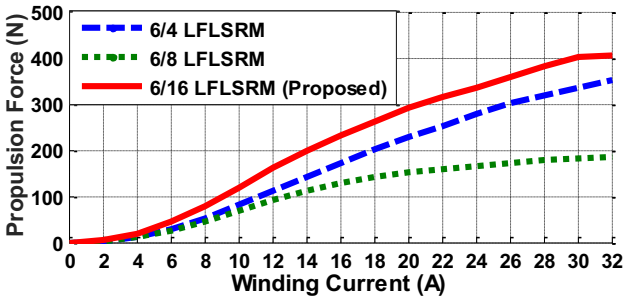

Figure 16. Force- current variation of the three motors.

increment between the non-aligned and aligned inductance line of the proposed motor as compared to the conventional LSRMs. This increment enhances the propulsion force produced by the motor as propulsion force directly depends upon the difference between aligned and non-aligned inductance as highlighted in Eq. (9).

Result shows that aligned flux of conventional LSRM starts saturating at much lower values of excitation currents as compared to that of the proposed LSRM. This assures the better flux accommodating capacity of the proposed LSRM that further increase its thrust generating capability. Figure 15 shows the flux distribution of all the three motors at aligned teeth positions. Proposed motor shows negligible saturation in the core at aligned position.

Figure 16 shows the plot of gross propulsion force with the increasing stator winding excitation current. From this result, it is clear that for same current excitation 6/16 LSRM produces higher propulsion force. The proposed LSRM shows satisfactory performance at winding excitation of 14A also, without any saturation in the cores.

Better flux performance is also the result of increased count of translator teeth, which has increased the stator slot breadth of the proposed motor. More slot area also allows for better cooling of the winding which reduces the slot insulation requirement of the windings. This characteristic makes it fit for the high-performance transit systems.

Table 10 gives the force characteristic comparison of the proposed LSRM with the conventional 6/4 and 6/8 LSRMs for the similar physical dimensions. The proposed 6/16 LSRM shows 53.23% and 99.5% increment in propulsion force as compared to 6/4 and 6/8 LSRMs, respectively. It also shows 39.84% and 14.6% reduction in force ripples as compared to 6/4 and 6/8 LSRM, respectively.

Figure 17 gives the comparison between force profiles of the three designed LSRMs. Improvement in the force profile of 6/16 LSRM is easily seen from this result.

To further test the force ripple reduction capability of the 6/16 LSRM, an equivalent 12/32 LSRM is designed by doubling the translator teeth and stator poles per phase in the 6/16 LSRM. Figure 18 gives the flux-density distribution of the two motors at aligned teeth position. The flux weakening is noticed in 12/32 LSRM due to poor overlapping between the teeth.

Table 10. Performance comparison of the three motors.

S. no.	Features	6/4 LSRM	6/8 LSRM	Proposed LSRM
1.	Gross propulsion force (N)	62.85	48.26	96.31
2.	Percentage ripple (%)	26.45	18.63	15.91

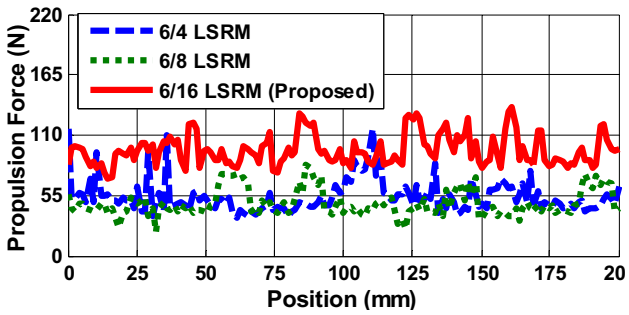

Figure 17. Propulsion force produced by the three motors.

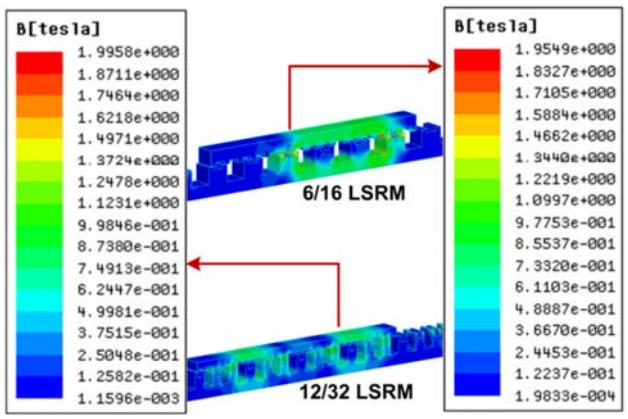

Figure 18. Flux density distribution at aligned teeth position.

Figure 19 shows the flux linkage and inductance waveforms in each phase of the proposed 6/16 LSRM and 12/32 LSRM. Splitting the teeth further into 12/32 configuration has decreased the rate of rise of inductance by approx. 50% that has decreased the average propulsion force of the motor.

Figure 20 shows the force performance comparison of the 12/32 configuration of 6/16 proposed LSRM.

Table 11 shows the comparative analysis of force performances of the 6/16 and 12/32 LSRM. Though the 12/32 configuration reduces the force ripples but it also reduces the force by 60.5%.

Therefore for transit applications, 6/16 LSRM configuration is the most feasible one among the studied motor configurations. Figure 21 shows the three phase excitation current profile used for exciting the 6/16 LSRM.

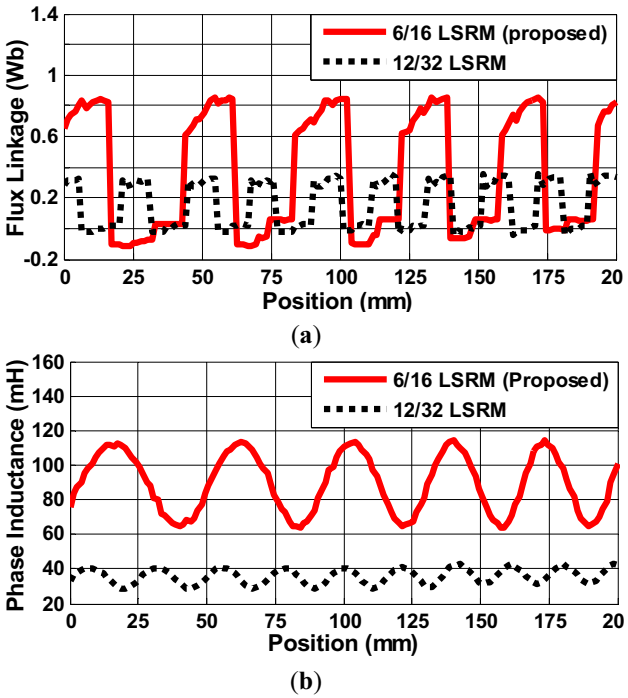

Figure 19. Comparative analysis (**a**) Phase flux linkages, (**b**) phase inductance.

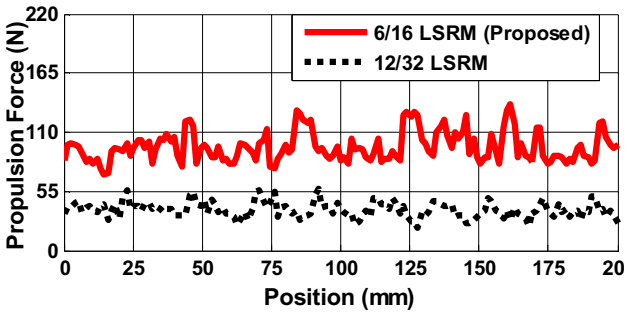

Figure 20. Propulsion force profiles of 6/16 and 12/32 LSRMs.

Table 11. Force performance comparison.

S. no.	Features	Proposed LSRM	12/32 LSRM
1.	Gross propulsion force (N)	96.31	38.04
2.	Percentage ripple (%)	15.91	11.10

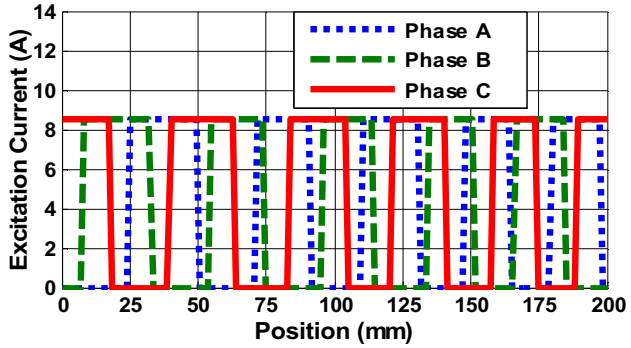

Figure 21. Three-phase excitation current for 6/16 LSRM.

5. Conclusion

This paper researched on a new split-teeth LSRM topology for direct force transmission with high-performance transit applications. The proposed motor carries the feature of having two-teeth in each stator pole with large number of translator poles than stator teeth, to enhance its force characteristics. The design of stator with split-teeth enhanced the force producing capability of the LSRM. Increased count of translator poles increased the slot area, which further helps in accommodating more copper if required. This further enabled the use of higher input current. The superiority of the proposed motor has been highlighted by comparing its performance with two 6/4 and 6/8 conventional LSRM with three-phase stationary stator configuration. The conventional motors are designed for similar physical dimensions for a fair comparison. The presented work used the FEA based analysis to study the force performances of these motors. The proposed motor shows higher propulsion force with lower saturations as compared with the conventional LSRMs. The force ripples reduction capability of the proposed motor is tested by comparing its performance by its equivalent 12/32 LSRM. This 12/32 LSRM is designed by doubling the translator teeth and stator poles per phase in the 6/16 LSRM. Additionally, in 6/16 LSRM the shape of the stator with more slot breadth has found convenient for forming stationary part in transit applications as this shape could increase the physical strength of the motor, ease of maintenance of the winding, improved natural cooling of the windings and prospective mass production. Therefore, the proposed motor shows its suitability for its use in upcoming transport systems.

List of symbols

V	Voltage per phase
R	Resistance per phase
i	Current per phase
ψ	Flux linkage per phase
N	Turns per phase
ø	Flux per phase
$ø_m$	Magnetizing flux
$ø_l$	Leakage flux
L	Winding inductance per phase
x	Translator position
v_s	Translator speed
P_m	Power generated by motor per phase
F_m	Genereated propulsion force
S_g	Air-gap reluctance
S_i	Iron path reluctance
S	Magnetic field path reluctance
l_i	Lengths of iron path
l_g	Lengths of air-gap
μ_r	Relative permittivity of the core material
μ_o	Permeability
L_s	Stack length
$l_{lap}(x)$	Overlap span between the translator and stator teeth
n	Stator teeth count per pole
A_i	Cross-sectional areas of iron-path
A_g	Cross-sectional areas of air-gap
S_{tw}	Breadth stator teeth
S_{sw}	Breadth stator slot
H_{ss}	Height Stator teeth
H_{sy}	Height stator yoke
S_{pp}	Pole-pitch stator
H_s	Height stator
t_t	Breadth translator teeth
t_s	Breadth translator slot
h_{ts}	Height translator teeth
h_{ty}	Height translator yoke
h_t	Height translator
t_{pp}	Pole-pitch translator
k_{sht}	Ratio between heights of stator notch and stator
k_{tht}	Ratio between heights of translator teeth and translator
k_{swd}	Ratio between breadths of stator notch and stator teeth
k_{twd}	Ratio between breadths of translator teeth and pole-pitch

References

[1] Zhou L and Shen Z 2011 Progress in high-speed train technology around the world. *Journal of ModernTransportation* 19: 1–6

[2] Lee H W, Kim K C and Lee J 2006 Review of maglev train technologies. *IEEE Transactions on Magnetics* 42: 1917–1925

[3] Uzuka T 2011 Trends in high-speed railways and the implications on power electronics and power devices. In: *IEEE 23rd International Symposium on Power Semiconductor Devices and ICs*, San Diego, CA, pp. 6–9

[4] Boldea I 2013 *Linear Electric Machines, Drives and Maglevs Handbook*. Boca Raton: CRC Press, pp 55–207

[5] Wang D H, Shao C L, Wang X H and Chen X J 2016 Design and performance comparison of a bilateral yokeless linear switched reluctance machine for urban rail transit system. In: *Vehicle Power and Propulsion Conference (VPPC)*, Hangzhou, pp. 1–5

[6] Wang D, Wang X and Du X F 2017 Design and comparison of a high force density dual-side linear switched reluctance motor for long rail propulsion application with low cost. *IEEE Transactions on Magnetics* 53: 1–4

[7] Liu C T, Su K S and Chen J W 2000 Operational stability enhancement analysis of a transverse flux linear switched-reluctance motor. *IEEE Transactions on Magnetics* 36: 3699–3702

[8] Krishnan R 2001 *Switched Reluctance Motor Drives*. Ed: Irwin J D. Boca Raton: CRC Press, pp 107–188

[9] Cao G, Fang J, Huang S, Duan J and Pan J F 2014 Optimization design of the planar switched reluctance motor on electromagnetic force ripple minimization. *IEEE Transactions on Magnetics* 50: 1–4

[10] Zou Y, Cheng K E, Cheung N C and Pan J 2014 Deformation and noise mitigation for the linear switched reluctance motor with skewed teeth structure. *IEEE Transactions on Magnetics* 50: 1–4

[11] Wang Y and Hao W 2018 Torque impulse balance control for multi-tooth fault tolerant switched-flux machines under open-circuit fault. *Energies* 11: 1–21

[12] Zhu J, Cheng K W E, Xue X and Zou Y 2017 Design of a new enhanced torque in-wheel switched reluctance motor with divided teeth for electric vehicles. *IEEE Transactions on Magnetics* 53: 1–4

[13] Prasad N, Jain S and Gupta S 2019 Design and analysis of a new improved force linear switched reluctance motor for transit application. *IETE Journal of Research*. https://doi.org/10.1080/03772063.2019.1676664